

Rate-Splitting Multiple Access for Integrated Sensing and Communications: A First Experimental Study

Xinze Lyu, *Student Member, IEEE*, Sundar Aditya, *Member, IEEE* and Bruno Clerckx, *Fellow, IEEE*

Abstract—A canonical use case of Integrated Sensing and Communications (ISAC) in multiple-input multiple-output (MIMO) systems involves a multi-antenna transmitter communicating with K users and sensing targets in its vicinity. For this setup, precoder and multiple access designs are of utmost importance, as the limited transmit power budget must be efficiently directed towards the desired directions (users and targets) to maximize both communications and sensing performance. This problem has been widely investigated analytically under various design choices, in particular (a) whether or not a dedicated sensing signal is needed, and (b) for different MIMO multiple access techniques, such as Space Division Multiple Access (SDMA) and Rate-Splitting Multiple Access (RSMA). However, a conclusive answer on which design choice achieves the best ISAC performance, backed by experimental results, remains elusive. We address this vacuum by experimentally evaluating and comparing RSMA and SDMA for communicating with two users ($K = 2$) and sensing (ranging) one target. Over three scenarios that are representative of *vehicular* ISAC, covering different levels of inter-user interference and separation/integration between sensing and communications, we show that RSMA without a dedicated sensing signal achieves better ISAC performance – i.e., higher sum throughput (upto 50% peak throughput gain) for similar radar SNR (between 20 to 24dB) – than SDMA with a dedicated sensing signal. This first-ever experimental study of RSMA ISAC demonstrates the feasibility and the superiority of RSMA for future multi-functional wireless systems.

Index Terms—Rate-Splitting Multiple Access (RSMA), Integrated Sensing and Communications (ISAC), RSMA prototyping, RSMA measurements

I. INTRODUCTION

Integrated Sensing and Communications (ISAC) is widely anticipated to be a prominent feature of future wireless networks, as evidenced by standardization activities on ISAC for 6G [1]. One strand of ISAC that has been extensively investigated by the research community is multiple-input multiple-output (MIMO) ISAC, as the MIMO paradigm is mature in both communications (comms) and radar [2]. In particular, a problem that has been widely investigated involves a multi-antenna transmitter (TX) simultaneously serving K comms users (UEs) and sensing targets in its vicinity. For this problem, the comms and sensing performance is closely linked to the amount of power radiated towards the UEs

and targets, respectively. As a result, the choice of precoders (beamforming) and multiple access techniques used at the TX has a direct bearing on ISAC performance. Indeed, in the context of ISAC, multiple access techniques make use of the resource dimensions (e.g., time, frequency, power, antenna, code, message, etc) to serve multiple physical users (communications) and virtual users (target to sense), ideally in the most efficient way [3].

The ISAC precoder design problem has been extensively studied to jointly optimize communication and sensing performance metrics in various well-motivated scenarios – conventional MIMO with fully digital beamforming [4], [5], [6], [7], [8], massive MIMO [9], [10], [11], [12], vehicular systems [13], [14], millimeter-wave with hybrid beamforming [15], [16], [17], [18], using low resolution analog-to-digital converters [19], etc. There are two implicit assumptions across these works. Firstly, they can all be viewed as adapting Space Division Multiple Access (SDMA) – the prevailing multiple access technique used in 5G – for ISAC, and secondly, they either assume a dedicated sensing signal [9], [12], [11], [15], or reuse comms signals¹ for sensing [5], [7], [8], [10], [13], [14], [16], [17], [18], [19] as pre-fixed design choices without scrutinizing the merits of each choice. As a result, two fundamental questions can be posed w.r.t the ISAC precoder design problem, namely:

- Q1. Are there alternatives to SDMA that could provide better ISAC performance²?
- Q2. Are separate signals needed for comms and sensing for the best ISAC performance?

These are especially pertinent questions, as specifications related to the waveform and multiple access technique are among the first to be decided in every new generation of standards.

Regarding Q1, Rate-Splitting Multiple Access (RSMA), which generalizes SDMA (and NOMA), has been shown both analytically and empirically to outperform SDMA (and NOMA) w.r.t comms [20], [21], [22]. Briefly, using RSMA to communicate with K UEs involves the design of $K + 1$ precoders to transmit $K + 1$ comms signals [22]. Likewise, using SDMA to communicate with K UEs and track a single target using a dedicated sensing signal also involves the design of $K + 1$ precoders³. These similarities strongly motivate an

This work was partially funded by UKRI Impact Acceleration Account (IAA) grant EP/X52556X/1 and UKRI grants EP/X040569/1, EP/Y037197/1, EP/X04047X/1, EP/Y037243/1.

X. Lyu, S. Aditya and B. Clerckx are with the Dept. of Electrical and Electronic Eng., Imperial College London, London SW7 2AZ, U.K. (e-mail: {x.lyu21, s.aditya, b.clerckx}@imperial.ac.uk).

¹By this, we mean the data payload comprising channel-coded and modulated symbols.

²See Definition 1 on page 6 for our definition of ISAC performance.

³Essentially, the target can be viewed as a virtual UE.

RSMA v/s SDMA ISAC comparison.

As for Q2, it is important to clarify what sensing entails. For instance, if the sensing task involves detecting the presence/absence of a target or direction finding, then clearly these can be accomplished using comms signals with an energy detection receiver or subspace methods like MUSIC, respectively. Importantly, the sensing signal processing for these tasks does not depend on the *content* of the comms signal. For target ranging (i.e., distance estimation) on the other hand, the signal content impacts estimation performance as the range estimator is a matched filter. Since the answer to Q2 is non-trivial for ranging, we choose this as the sensing task in this paper, although the terms sensing and ranging shall be used interchangeably. However, it has been shown that the ranging performance of comms signals matches that of dedicated sensing signals – e.g., frequency modulated continuous wave (FMCW) – asymptotically at large signal lengths [23].

Taken together, Q1 and Q2 motivate the following four-way ISAC comparison – RSMA/SDMA with/without dedicated sensing signal. This has been investigated in [24], [25], [26], [27], [28] with link-level simulations indicating that RSMA without a dedicated sensing signal achieves the best ISAC performance – intuitively, the *extra* precoder (i.e., $K + 1$ precoders for K UEs) can be used for sensing⁴. In particular, [24] was the first to theoretically show that RSMA can be used for the dual purpose of boosting the communication sum rate of multiple users and simultaneously increasing the sensing performance, hence enlarging the communication-sensing performance trade-off. This is due to the common streams in RSMA that can be used to manage inter-user interference and sensing targets. However, a conclusive answer on which design choice achieves the best ISAC performance, backed by experimental results, is missing in the literature – experimental evaluations of ISAC for single-antenna systems is presented in [29], [30], [31] and for multi-antenna ISAC (SDMA) in [32]. In this paper, we address this void, and our contributions are as follows:

- We formulate a signal model for RSMA ISAC with a dedicated sensing signal, which includes the other design choices (SDMA ISAC, RSMA ISAC without a dedicated sensing signal) as special cases. We then use the sum throughput (comms metric) and radar SNR (sensing metric) to define an *ISAC performance region* to compare the different design choices.
- Using software-defined radios (SDRs), we implement the above signal model using OFDM signals largely based on IEEE 802.11ac-VHT physical layer frames [33]. We consider a signal bandwidth of 100MHz, yielding a range resolution (bin size) of 1.5m.
- In our measurements, we consider three scenarios that are representative of *vehicular ISAC*, covering different levels of inter-user interference and separation/integration between sensing and communications. Over these scenarios, we observe that:

- a) The SDMA ISAC performance boundary lies in the interior of the RSMA ISAC performance region. Hence, RSMA ISAC outperforms SDMA ISAC.
- b) Moreover, the RSMA ISAC performance boundary is achieved *without a dedicated sensing signal*. In contrast, a dedicated sensing signal is needed to achieve the SDMA performance boundary.
- c) The gap between the SDMA and RSMA ISAC performance regions is scenario dependent. In particular, RSMA without a dedicated sensing signal can achieve peak sum throughput gains of upto 50% over SDMA with a dedicated sensing signal, for similar radar SNR (between 20 and 24dB).

A. Organization

The rest of this paper is organized as follows. In Section II, we describe the signal model for RSMA ISAC with a dedicated sensing signal; the other design choices are special cases of this general case (see Section II-C). In Section III, we present details of our SDR-based RSMA ISAC prototype, specifically the control signaling, OFDM payload structure, MCS levels etc. In Section IV-A, we motivate our measurement scenarios that are representative of vehicular ISAC. Capturing the peak performance of RSMA ISAC with a dedicated sensing signal involves a four-dimensional parameter search, which is cumbersome to realize in an experimental setting. This motivates us to pursue *simulation-aided parameter search*, described in Section IV-B, whereby we obtain a subset of well-chosen parameters that we use to measure and compare the ISAC performance of RSMA and SDMA, the results of which are presented in Section IV-C. Finally, Section V concludes the paper.

B. Notation

Column vectors are represented by lowercase bold letters (e.g., \mathbf{h}). $\mathbf{1}$ denotes the all-one vector, $|\cdot|$ the magnitude of scalars, $(\cdot)^H$ the Hermitian operator, $\|\cdot\|$ the Euclidean norm, and $\mathcal{CN}(0, \sigma^2)$ the circularly symmetric complex Gaussian distribution with zero mean and variance σ^2 . For a uniform linear array with N_T antenna elements and half-wavelength spacing, $\mathbf{a}_\theta = [1 \ e^{j\pi \sin \theta} \ \dots \ e^{j\pi(N_T-1) \sin \theta}]^T$ denotes the steering vector along direction θ .

II. SYSTEM MODEL

Consider a TX with N_T antennas serving two-single antenna UEs and sensing (ranging) one target at its broadside as a monostatic radar in tracking mode. We consider OFDM signals over N_c subcarriers for both comms and sensing.

A. Transmit signal

a) *RSMA comms*: For the two-UE case, RSMA comms involves the transmission of three linearly precoded signals [22]. Specifically, let W_i denote the message meant for UE i ($= 1, 2$). At the TX, each W_i is split into common and private portions – denoted by $W_{c,i}$ and $W_{p,i}$, respectively. The common portions, $W_{c,1}$ and $W_{c,2}$, are combined into a

⁴This works only because the comms signal carried by the precoder can also be used for sensing. Thus, Q1 and Q2 in page 1 are closely related questions.

common message, which is then encoded and modulated to form a *common stream*, $s_c[k]$ ($k = 0, \dots, N_c - 1$) over the subcarriers. Similarly, $W_{p,1}$ and $W_{p,2}$ are individually encoded and modulated to form *private streams*, $s_1[k]$ and $s_2[k]$, respectively. We assume zero-mean, unit-energy symbols for each stream. The three streams are then linearly precoded before transmission.

Remark 1 (SDMA as a special case of RSMA). *In the absence of message splitting (i.e., no s_c), RSMA reduces to SDMA.*

b) *Sensing (Ranging)*: Ranging as a stand-alone functionality can be realized by transmitting a deterministic *sensing signal*, $s_r[k]$, aimed at the target using a precoder (beam-former) \mathbf{p}_r .

c) *RSMA ISAC*: From a) and b) above, the RSMA ISAC transmit signal, $\mathbf{x}[k]$, can be modeled as follows:

$$\mathbf{x}[k] = \mathbf{p}_c[k]s_c[k] + \mathbf{p}_1[k]s_1[k] + \mathbf{p}_2[k]s_2[k] + \mathbf{p}_r[k]s_r[k], \quad (1)$$

where for subcarrier k , $\mathbf{p}_c[k]$ is referred to as the *common stream precoder*, $\mathbf{p}_i[k]$ the *private stream precoder* for UE i , and $\mathbf{p}_r[k]$ the *sensing precoder*. We assume a sum transmit power constraint, i.e.,

$$\sum_{k=0}^{N_c-1} (\|\mathbf{p}_c[k]\|^2 + \|\mathbf{p}_1[k]\|^2 + \|\mathbf{p}_2[k]\|^2 + \|\mathbf{p}_r[k]\|^2) = P_T \quad (2)$$

Remark 2 (Ranging using comms signals). *To use the comms signals – $s_c[\cdot]$, $s_1[\cdot]$ and $s_2[\cdot]$ – for ranging [23], the respective precoders – $\mathbf{p}_c[\cdot]$, $\mathbf{p}_1[\cdot]$ and $\mathbf{p}_2[\cdot]$ – should strike a balance between radiating power towards the desired UE(s) and the target. This trade-off motivates our precoder design choices in the next subsection.*

B. Precoder Design

Let $\mathbf{h}_i[k] \in \mathbb{C}^{N_T}$ denote the slowly varying, flat fading (comms) channel between the TX and UE i ($i = 1, 2$). Through downlink pilot signals, we assume UE i obtains an estimate of $\mathbf{h}_i[k]$, denoted by $\hat{\mathbf{h}}_i[k]$, which is fed back to the TX. Let $\mathbf{u}_i[k] := \hat{\mathbf{h}}_i[k]/\|\hat{\mathbf{h}}_i[k]\|$ denote the unit vector along $\hat{\mathbf{h}}_i[k]$. Similarly, let $\mathbf{u}_0 := \mathbf{a}_0/\sqrt{N_T}$ denote the normalized steering vector along the TX's broadside, which is assumed to be the target direction.

a) *Design of $\mathbf{p}_c[\cdot]$* : In RSMA comms, each UE independently decodes $s_c[\cdot]$ first by treating the interference from $s_1[\cdot]$ and $s_2[\cdot]$ as noise. Hence, $\mathbf{p}_c[\cdot]$ must have sufficient gain at both UEs (for comms), as well as the target direction (for sensing, see Remark 2). This motivates a weighted maximum ratio transmission (MRT) precoder choice for $\mathbf{p}_c[\cdot]$, as follows:

$$\mathbf{p}_c[k] = \sqrt{P_T t_{\text{comms}} (1 - t_p)} \times \frac{(\sqrt{\alpha_c} \mathbf{u}_c[k] + \sqrt{1 - \alpha_c} \mathbf{u}_0)}{\sqrt{\sum_{k'=0}^{N_c-1} \|\sqrt{\alpha_c} \mathbf{u}_c[k'] + \sqrt{1 - \alpha_c} \mathbf{u}_0\|^2}}, \quad (3)$$

where

$$\mathbf{u}_c[k] = (\mathbf{u}_1[k] + \mathbf{u}_2[k]) / \|\mathbf{u}_1[k] + \mathbf{u}_2[k]\|. \quad (4)$$

In (4), through equi-weighted MRT along $\hat{\mathbf{h}}_1[k]$ and $\hat{\mathbf{h}}_2[k]$, the vector $\mathbf{u}_c[k]$ ensures some gain at both UEs, and the form of (3) further ensures some gain along the target direction (\mathbf{u}_0) as well. The parameter $\alpha_c \in [0, 1]$ captures the priority/weight assigned to comms. Finally, $t_{\text{comms}} \in [0, 1]$ captures the fraction of the transmit power allocated for comms, and $t_p \in [0, 1]$ represents the fraction of t_{comms} that is allocated to the private stream precoders.

b) *Design of $\mathbf{p}_i[\cdot]$ ($i = 1, 2$)*: After decoding $s_c[\cdot]$, UE i subtracts its contribution (i.e., through successive interference cancellation) and then decodes $s_i[\cdot]$ by treating the interference from the other private stream as noise. Hence, $\mathbf{p}_i[\cdot]$ must have sufficient gain at UE i as well as the target direction. This motivates the following weighted MRT precoder choice for $\mathbf{p}_i[\cdot]$ similar to (3):

$$\mathbf{p}_i[k] = \sqrt{\frac{P_T t_{\text{comms}} t_p}{2}} \times \frac{(\sqrt{\alpha_p} \mathbf{u}_i[k] + \sqrt{1 - \alpha_p} \mathbf{u}_0)}{\sqrt{\sum_{k'=0}^{N_c-1} \|\sqrt{\alpha_p} \mathbf{u}_i[k'] + \sqrt{1 - \alpha_p} \mathbf{u}_0\|^2}}, \quad (5)$$

where like α_c in (3), $\alpha_p \in [0, 1]$ captures the priority/weight assigned to comms. In general, $\alpha_c \neq \alpha_p$. We further assume that the total private stream precoder power ($= t_{\text{comms}} t_p$) is equally divided between $\mathbf{p}_1[\cdot]$ and $\mathbf{p}_2[\cdot]$. This is a reasonably good choice when the UEs have similar channel strengths (i.e., $\|\hat{\mathbf{h}}_1\| \approx \|\hat{\mathbf{h}}_2\|$), which is the scenario we focus on in our measurements.

c) *Design of $\mathbf{p}_r[\cdot]$* : Since $s_r[\cdot]$ is not an information-bearing signal, $\mathbf{p}_r[\cdot]$ needs to have high gain only along the target direction. From (3) and (5), $1 - t_{\text{comms}}$ is the fraction of the transmit power allocated solely for sensing. Hence,

$$\mathbf{p}_r[k] = \sqrt{\frac{P_T (1 - t_{\text{comms}})}{N_c}} \times \mathbf{u}_0. \quad (6)$$

Remark 3. *Four parameters are used to capture the full extent of the comms-sensing trade-off in (3)-(6). In summary, they are:*

- $t_{\text{comms}} \in [0, 1]$: *Fraction of transmit power allocated for comms. $t_{\text{comms}} \rightarrow 0/1$ implies most of the power allocated for sensing/comms.*
- $t_p \in [0, 1]$: *Fraction of comms power (i.e., t_{comms}) allocated to the private streams allocated for comms. $t_p \rightarrow 0/1$ implies most of t_{comms} is allocated to the common/private stream(s).*
- $\alpha_c \in [0, 1]$: *As $\mathbf{p}_c[\cdot]$ can be used for both comms and sensing whenever it is allocated non-zero power, α_c is the priority given to comms. In particular, $\alpha_c \rightarrow 0/1$ implies very high priority given to sensing/comms.*
- $\alpha_p \in [0, 1]$: *Like α_c , α_p is the priority given to comms for the private stream precoders, $\mathbf{p}_1[\cdot]$ and $\mathbf{p}_2[\cdot]$. Again, $\alpha_p \rightarrow 0/1$ implies very high priority given to sensing/comms.*

Remark 4 (Heuristic precoders). *The precoders in (3)-(6) are sub-optimal, as they are not obtained by optimizing any performance metrics (e.g., sum throughput for comms, SNR of radar return for sensing). However, they are still useful because they are easy to implement, which in turn makes it relatively easier to obtain an **empirical ISAC performance region** (e.g., the achievable pairs of sum throughput and radar SNR – see Definition 1 in page 6 for a precise definition) to judge the comms/sensing trade-off associated with each design choice (i.e., RSMA/SDMA with/without dedicated signal). Nevertheless, the suboptimality of the precoders means that the gap between the different ISAC performance region boundaries could potentially be enlarged through optimized precoders. This is left for future work.*

Next, we focus on some special cases of (3)-(6) that are of interest.

C. Special Cases

1) *RSMA ISAC without dedicated sensing signal – the general case:* A key feature of (3)-(6) is the fact that comms precoders can be used for sensing, but not vice-versa, as $s_r[\cdot]$ offers no comms benefit. Hence, it is reasonable to question whether the power allocated power to a dedicated sensing signal/precoder could be diverted to comms to significantly enhance comms performance, with minimal loss in sensing performance? To investigate this, t_{comms} can be set to 1 on (3)-(6) to yield an RSMA ISAC transmit signal involving three precoders, where each precoder is beneficial for both comms and sensing.

2) *RSMA ISAC without dedicated sensing signal – a soft sensing/comms separation:* While all precoders are beneficial for both comms and sensing in the previous special case, a balance can be struck wherein some of them prioritize sensing more than comms, while the others achieve the opposite effect. This can be realized, for instance, by setting $\alpha_c = 1 - \alpha_p$, where $\alpha_p \in [1/2, 1)$ (in addition to $t_{\text{comms}} = 1$). Thus, the private stream precoders prioritize comms, while the common stream precoder prioritizes sensing, similar to [27]. In this way, a soft separation of comms/sensing functionality for the precoders can be realized.

3) *SDMA ISAC with dedicated sensing signal – the general case:* With a dedicated sensing signal, $t_{\text{comms}} < 1$. Furthermore, from Remark 1, it follows that SDMA can be realized by setting $t_p = 1$.

4) *SDMA ISAC with dedicated sensing signal – a hard sensing/comms separation:* With a dedicated sensing signal/precoder, perhaps the comms precoder should *solely* prioritize comms to significantly enhance comms performance, with minimal loss in sensing performance? This amounts to a *hard* comms/sensing separation among the precoders, in contrast to the soft separation from special case no. 2. This can be realized by setting $\alpha_p = 1$ (in addition to $t_{\text{comms}} < 1, t_p = 1$).

5) *SDMA ISAC without dedicated sensing signal:* Finally, this special case can be realized by setting $t_{\text{comms}} = 1$ and $t_p = 1$, giving rise to an SDMA ISAC transmit signal involving two precoders, each of which is beneficial for both comms and sensing.

Table I summarizes the special cases described above⁵. Next, we introduce the performance metrics for comms and sensing performance and define the ISAC performance region to quantify ISAC performance.

D. Performance Metrics

Let $\mathbf{P} := \{\mathbf{p}_c[k], \mathbf{p}_1[k], \mathbf{p}_2[k], \mathbf{p}_r[k] : \forall k\}$ denote the collection of precoders.

a) *Comms:* In our measurements, the comms performance metric is the *MCS-limited sum throughput*. An MCS level is characterized by a pair (m, r) , where positive integer m denotes the bits per constellation symbol (e.g., 1 for BPSK) and $r \in (0, 1]$ denotes the code rate.

Remark 5 (Necessary condition for decoding MCS level (m, r)). *An OFDM symbol stream over N_c subcarriers encoded using (m, r) can be successfully decoded at a UE only if*

$$\frac{1}{N_c} \sum_{k=0}^{N_c-1} \log_2(1 + \text{SINR}[k]) \geq mr \quad (7)$$

where $\text{SINR}[k]$ denotes the signal-to-interference-plus-noise ratio of the symbol stream at subcarrier k at the UE.

The above inequality is a **necessary, but not sufficient condition** for successfully decoding (m, r) . This is because the left hand side represents the spectral efficiency (in bits/s/Hz) that can be achieved through Gaussian encoding, whereas the right hand side is the spectral efficiency achievable using (m, r) , which typically involves encoding over the binary field and modulation over discrete (non-Gaussian) constellations. Due to this mismatch, the minimum SNR needed to decode (m, r) is usually higher than that given by (7) – typically modeled as a < 2 dB penalty [34].

Successful decoding of (m, r) yields a throughput (measured in bits/s) of Bmr , where B denotes the signal bandwidth (after accounting for signaling overheads, such as cyclic prefix).

The received signal, $y_i[k]$, at the i -th UE given by:

$$\begin{aligned} y_i[k] &= \mathbf{h}_i^H[k] \mathbf{x}[k] + n_i[k] \quad (i = 1, 2) \\ &= \mathbf{h}_i^H[k] \mathbf{p}_r[k] s_r[k] + \mathbf{h}_i^H[k] \mathbf{p}_c[k] s_c[k] \\ &\quad + \mathbf{h}_i^H[k] \mathbf{p}_1[k] s_1[k] + \mathbf{h}_i^H[k] \mathbf{p}_2[k] s_2[k] + n_i[k] \end{aligned} \quad (8)$$

We assume $s_r[\cdot]$ is known at the UEs and can be subtracted before decoding $s_c[\cdot]$, $s_1[\cdot]$ and $s_2[\cdot]$. Let $\mathcal{M} = \{(m_c, r_c), (m_1, r_1), (m_2, r_2)\}$ denote the MCS levels chosen for $(s_c[\cdot], s_1[\cdot], s_2[\cdot])$, respectively. After subtracting $s_r[\cdot]$, each UE independently decodes $s_c[\cdot]$, while treating the interference from $s_1[\cdot]$ and $s_2[\cdot]$ as noise. Thus, from Remark 5, the

⁵NOMA is a subset of RSMA obtained by switching off one private stream [22]. However, NOMA ISAC is not evaluated in this paper since it has been shown to provide the lowest ISAC performance in the three-way cross-comparison with SDMA ISAC and RSMA ISAC theoretically [27], [28], and lower throughput performance experimentally [20].

Spl. case	Scheme	Parameters	Precoders	Comments
1.	RSMA ISAC w/o dedicated sensing signal – the general case	$t_{\text{comms}} = 1$ $\alpha_c \in [0, 1]$ $\alpha_p \in [0, 1]$ $t_p \in [0, 1]$	$\mathbf{p}_c[k] = \sqrt{P_T(1-t_p)} \times \frac{\sqrt{\alpha_c \mathbf{u}_c[k] + \sqrt{1-\alpha_c} \mathbf{u}_0}}{\sqrt{\sum_{k'} \ \sqrt{\alpha_c} \mathbf{u}_c[k'] + \sqrt{1-\alpha_c} \mathbf{u}_0\ ^2}}$ $\mathbf{p}_1[k] = \sqrt{P_T \frac{t_p}{2}} \times \frac{\sqrt{\alpha_p \mathbf{u}_1[k] + \sqrt{1-\alpha_p} \mathbf{u}_0}}{\sqrt{\sum_{k'} \ \sqrt{\alpha_p} \mathbf{u}_1[k'] + \sqrt{1-\alpha_p} \mathbf{u}_0\ ^2}}$ $\mathbf{p}_2[k] = \sqrt{P_T \frac{t_p}{2}} \times \frac{\sqrt{\alpha_p \mathbf{u}_2[k] + \sqrt{1-\alpha_p} \mathbf{u}_0}}{\sqrt{\sum_{k'} \ \sqrt{\alpha_p} \mathbf{u}_2[k'] + \sqrt{1-\alpha_p} \mathbf{u}_0\ ^2}}$	$\mathbf{u}_c[k] = (\mathbf{u}_1[k] + \mathbf{u}_2[k]) / \ \mathbf{u}_1[k] + \mathbf{u}_2[k]\ $. See Section II-C1. No dedicated radar signal/precoder. In general, common and pvt. streams have different priorities for comms/sensing (i.e., $\alpha_c \neq \alpha_p$).
2.	RSMA ISAC w/o dedicated sensing signal – a soft sensing/comms separation	$t_{\text{comms}} = 1$ $\alpha_c = 1 - \alpha_p$ $\alpha_p \in [1/2, 1]$ $t_p \in [0, 1]$	$\mathbf{p}_c[k] = \sqrt{P_T(1-t_p)} \times \frac{\sqrt{1-\alpha_p} \mathbf{u}_c[k] + \sqrt{\alpha_p} \mathbf{u}_0}{\sqrt{\sum_{k'} \ \sqrt{1-\alpha_p} \mathbf{u}_c[k'] + \sqrt{\alpha_p} \mathbf{u}_0\ ^2}}$ $\mathbf{p}_1[k] = \sqrt{P_T \frac{t_p}{2}} \times \frac{\sqrt{\alpha_p \mathbf{u}_1[k] + \sqrt{1-\alpha_p} \mathbf{u}_0}}{\sqrt{\sum_{k'} \ \sqrt{\alpha_p} \mathbf{u}_1[k'] + \sqrt{1-\alpha_p} \mathbf{u}_0\ ^2}}$ $\mathbf{p}_2[k] = \sqrt{P_T \frac{t_p}{2}} \times \frac{\sqrt{\alpha_p \mathbf{u}_2[k] + \sqrt{1-\alpha_p} \mathbf{u}_0}}{\sqrt{\sum_{k'} \ \sqrt{\alpha_p} \mathbf{u}_2[k'] + \sqrt{1-\alpha_p} \mathbf{u}_0\ ^2}}$	See Section II-C2. A special case of 1 above, where a soft sensing/comms separation is realized through the common (private) stream precoder(s) prioritizing sensing (comms).
3.	SDMA ISAC with dedicated sensing signal – the general case	$t_{\text{comms}} \in (0, 1)$ $t_p = 1$ $\alpha_p \in (0, 1)$	$\mathbf{p}_1[k] = \sqrt{P_T \frac{t_{\text{comms}}}{2}} \times \frac{\sqrt{\alpha_p} \mathbf{u}_1[k] + \sqrt{1-\alpha_p} \mathbf{u}_0}{\sqrt{\sum_{k'} \ \sqrt{\alpha_p} \mathbf{u}_1[k'] + \sqrt{1-\alpha_p} \mathbf{u}_0\ ^2}}$ $\mathbf{p}_2[k] = \sqrt{P_T \frac{t_{\text{comms}}}{2}} \times \frac{\sqrt{\alpha_p} \mathbf{u}_2[k] + \sqrt{1-\alpha_p} \mathbf{u}_0}{\sqrt{\sum_{k'} \ \sqrt{\alpha_p} \mathbf{u}_2[k'] + \sqrt{1-\alpha_p} \mathbf{u}_0\ ^2}}$ $\mathbf{p}_r[k] = \sqrt{P_T \frac{(1-t_{\text{comms}})}{N_c}} \times \mathbf{u}_0$	See Section II-C3. There exists a dedicated radar signal/precoder, but the comms precoders also have some priority for sensing.
4.	SDMA ISAC with dedicated sensing signal – a hard sensing/comms separation	$t_{\text{comms}} \in (0, 1)$ $t_p = 1$ $\alpha_p = 1$	$\mathbf{p}_1[k] = \sqrt{P_T \frac{t_{\text{comms}}}{2}} \times \mathbf{u}_1[k]$ $\mathbf{p}_2[k] = \sqrt{P_T \frac{t_{\text{comms}}}{2}} \times \mathbf{u}_2[k]$ $\mathbf{p}_r[k] = \sqrt{P_T \frac{(1-t_{\text{comms}})}{N_c}} \times \mathbf{u}_0$	See Section II-C4. A special case of 3 above, where the comms precoders do not prioritize sensing. Thus, a hard sensing/comms separation is realized.
5.	SDMA ISAC w/o dedicated sensing signal	$t_{\text{comms}} = 1$ $t_p = 1$ $\alpha_p \in (0, 1)$	$\mathbf{p}_1[k] = \sqrt{\frac{P_T}{2}} \times \frac{\sqrt{\alpha_p} \mathbf{u}_1[k] + \sqrt{1-\alpha_p} \mathbf{u}_0}{\sqrt{\sum_{k'} \ \sqrt{\alpha_p} \mathbf{u}_1[k'] + \sqrt{1-\alpha_p} \mathbf{u}_0\ ^2}}$ $\mathbf{p}_2[k] = \sqrt{\frac{P_T}{2}} \times \frac{\sqrt{\alpha_p} \mathbf{u}_2[k] + \sqrt{1-\alpha_p} \mathbf{u}_0}{\sqrt{\sum_{k'} \ \sqrt{\alpha_p} \mathbf{u}_2[k'] + \sqrt{1-\alpha_p} \mathbf{u}_0\ ^2}}$	See Section II-C5. No dedicated radar signal/precoder

TABLE I: List of special cases described in Section II-C.

maximum MCS-limited common stream throughput, denoted by $T_c(\mathbf{P})$, is given by:

$$T_c(\mathbf{P}) = \max_{\mathcal{M} \in \mathbb{M}} Bm_c r_c \quad (9)$$

$$\text{s.t. } \min_i \frac{1}{N_c} \sum_{k=0}^{N_c-1} \log_2(1 + \text{SINR}_{c,i}[k; \mathbf{P}]) > m_c r_c, \quad (10)$$

where (i) \mathbb{M} denotes the collection of permissible MCS levels for the three streams, which is typically pre-determined through standards (see Table III for the \mathbb{M} used in our measurements), (ii) $\text{SINR}_{c,i}[k; \mathbf{P}]$ denotes the common stream SINR at the k -th subcarrier at UE i , which is a function of \mathbf{P} as follows:

$$\text{SINR}_{c,i}[k; \mathbf{P}] = \frac{|\mathbf{h}_i^H[k] \mathbf{p}_c[k]|^2}{\sum_{j=1}^2 |\mathbf{h}_i^H[k] \mathbf{p}_j[k]|^2 + \sigma^2}. \quad (11)$$

The minimum in (10) is due to both UEs needing to decode $s_c[\cdot]$. Furthermore, $T_c(\mathbf{P}) = 0$ when (10) is not satisfied even for the lowest MCS level.

After decoding $s_c[\cdot]$ and subtracting its contribution from $y_i[\cdot]$, UE i decodes $s_i[\cdot]$ while treating the interference from the other private stream ($s_j[\cdot]$, $j \neq i$) as noise. Similar to

$T_c(\mathbf{P})$, the maximum MCS-limited private stream throughput at UE i , denoted by $T_i(\mathbf{P})$, is given by:

$$T_i(\mathbf{P}) := \max_{\mathcal{M} \in \mathbb{M}} Bm_i r_i \quad (12)$$

$$\text{s.t. } \frac{1}{N_c} \sum_{k=0}^{N_c-1} \log_2(1 + \text{SINR}_{p,i}[k; \mathbf{P}]) > m_i r_i, \quad (13)$$

where $\text{SINR}_{p,i}[k; \mathbf{P}]$ denotes the private stream SINR at the k -th subcarrier for the i -th UE, which is a function of \mathbf{P} as follows:

$$\text{SINR}_{p,i}[k; \mathbf{P}] = \frac{|\mathbf{h}_i[k]^H \mathbf{p}_i[k]|^2}{|\mathbf{h}_i[k]^H \mathbf{p}_j[k]|^2 + \sigma^2} \quad (j \neq i). \quad (14)$$

From (9)-(13), the MCS-limited sum throughput, $T_{\text{sum}}(\mathbf{P})$, has the following expression:

$$T_{\text{sum}}(\mathbf{P}) = T_c(\mathbf{P}) + \mathbb{1}(T_c(\mathbf{P}) > 0)(T_1(\mathbf{P}) + T_2(\mathbf{P})). \quad (15)$$

Remark 6 (Impact of Imperfect SIC and Finite MCS levels). *The indicator function in (15) captures the impact of imperfect SIC and finite MCS levels – i.e., if a UE cannot decode the common stream at the lowest MCS level, then it cannot decode its private stream at any MCS level, resulting in zero throughput. If at least one UE experiences such a **throughput collapse**, then RSMA is not viable (under the constraint of*

finite MCS levels), and we assume $T_{\text{sum}}(\mathbf{P}) = 0$. This phenomenon was experimentally observed in [35].

It is worth noting that this is a marked departure from standard analytical models that assume perfect SIC and infinitely many MCS levels of arbitrary granularity (implicit when Gaussian encoding is assumed). Under these assumptions, the highest achievable RSMA sum throughput is never smaller than the highest achievable SDMA sum throughput [36]. However, with finite MCS levels, the SDMA sum throughput can exceed the RSMA sum throughput, especially when the common stream precoder is not allocated enough power to decode the lowest MCS level.

Remark 7 (SDMA Sum Throughput). *Since there is no common stream in SDMA (see Remark 1), the maximum MCS-limited SDMA sum throughput equals $T_1(\mathbf{P}) + T_2(\mathbf{P})$, where $\mathcal{M} = \{(m_1, r_1), (m_2, r_2)\}$.*

Remark 8 (Upper bound on measured throughputs). *Since (10) and (13) are necessary but not sufficient conditions for decoding non-Gaussian constellations (see Remark 5), $T_c(\mathbf{P})$, $T_i(\mathbf{P})$ ($i = 1, 2$) and $T_{\text{sum}}(\mathbf{P})$ are upper bounds for the measured common stream, private stream and sum throughputs, respectively.*

b) Ranging: In our measurements, performance metric for ranging is the *post-processing radar SNR*. We consider a single-antenna radar receiver (RX) colocated with the TX. For transmit signal $\mathbf{x}[k]$ given by (1), the signal at the radar RX, denoted by $y_r[k]$, is given by:

$$y_r[k] = \beta(\mathbf{a}_0^H \mathbf{x}[k]) \exp\left(j2\pi \frac{n_0}{N_c} k\right) + n_r[k], \quad (16)$$

where β denotes the signal attenuation, n_0 is the time domain sample delay, and $n_r[k] \sim \mathcal{CN}(0, \sigma_r^2)$ the RX noise. The maximum likelihood estimate of n_0 , denoted by \hat{n}_0 , is given by:

$$\hat{n}_0 = \arg \max_n |Y_r[n]|, \quad (17)$$

$$\text{where } Y_r[n] = \sum_{k=0}^{N_c-1} y_r[k] (\mathbf{x}^H[k] \mathbf{a}_0) \exp\left(-j2\pi \frac{n}{N_c} k\right). \quad (18)$$

In (18), $Y_r[n]$ ($n = 0, \dots, N_c - 1$) is the N_c -point DFT of $\{y_r[k] (\mathbf{x}^H[k] \mathbf{a}_0) : k = 0, \dots, N_c - 1\}$ delayed by n samples, and (17) amounts to identifying the location of the DFT peak.

The post-processing radar SNR, denoted by $\text{SNR}_{\text{rad}}(\mathbf{P})$, is defined as follows:

$$\text{SNR}_{\text{rad}}(\mathbf{P}) = \frac{|Y_r[\hat{n}_0]|^2}{\frac{1}{N_c-1} \sum_{n \neq \hat{n}_0} |Y_r[n]|^2} \quad (19)$$

The right-hand side of (19) is a function of \mathbf{P} , since $Y_r[\cdot]$ in (18) is a function of $\mathbf{x}[k]$, which in turn is a function of \mathbf{P} (see (1)).

Definition 1 (RSMA ISAC performance region). *The ordered pair $(T_{\text{sum}}(\mathbf{P}), \text{SNR}_{\text{rad}}(\mathbf{P}))$ captures RSMA ISAC performance. Specifically, the four parameters – $(t_{\text{comms}}, t_p, \alpha_c, \alpha_p)$ – uniquely determine \mathbf{P} (see (3)-(6) and Remark 3), which*

	Name	Description
1.	Workstation	Running LabVIEW NXG
2.	NI USRP-2942 (3 units)	SDRs used to realize TX, UEs and radar RX
3.	NI CPS-8910	Provides additional PCIe ports
4.	NI CDA-2990	8 Channel, 10MHz clock distribution device
5.	Patch antennas (non-commercial, designed in house)	TX antennas
6.	TP-Link TL-ANT2405C (3 units)	Anchor and (two) UE antennas
7.	MM-ANT-NF-5G Yagi antenna	Radar RX antenna

TABLE II: List of hardware components in our RSMA prototype.

in turn determines $(T_{\text{sum}}(\mathbf{P}), \text{SNR}_{\text{rad}}(\mathbf{P}))$. Thus, the set of all feasible values for the four parameters corresponds to a collection of points $(T_{\text{sum}}(\mathbf{P}), \text{SNR}_{\text{rad}}(\mathbf{P}))$, which we define as the RSMA ISAC performance region, whose boundary (Pareto frontier) captures the limits of achievable ISAC performance for the heuristic precoders given by (3)-(6) – see also Remark 4.

Remark 9. *Along the lines of Definition 1, the ISAC performance region can be defined for each of the special cases in Table I. By definition, these performance regions are contained within the RSMA ISAC performance region defined above. However, the following questions are of particular interest:*

- *Can the boundary of the RSMA ISAC performance region in Definition 1 be achieved by one or more of the special cases in Table I?*
- *How do the boundaries of the SDMA and RSMA ISAC performance regions w.r.t to one another?*

Before addressing the questions in the previous remark in Section IV, we first describe our RSMA ISAC prototype in the following section.

III. RSMA ISAC PROTOTYPE

Fig. 1 depicts the RSMA ISAC block diagram, which we implement using software-defined radios (SDR). The TX, UEs and the radar RX are realized using National Instruments' (NI) USRP 2942 SDR units, which have two antennas/RF chains. Hence, we use three USRP 2942 units – one to realize the two-antenna TX, another to realize two single-antenna UEs, and a third to realize the (single-antenna) radar RX, where we use a Yagi-antenna pointing towards the target to obtain a strong radar return and suppress some of the self-interference (SI) from the TX \rightarrow radar RX direct path. The TX and the radar RX are situated close together to mimic a monostatic configuration. The USRPs share a common timing source (NI CDA-2990), and are controlled by a workstation running LabVIEW NXG, through which the various blocks in Fig. 1 are realized. All connections (SDRs to workstation, SDRs to timing sources) are through PCIe cables, facilitated by a PCIe bus (NI CPS-8910). A list of hardware components is provided in Table II.

We realize the following two-stage protocol to implement the system model described in Section II, adopting several

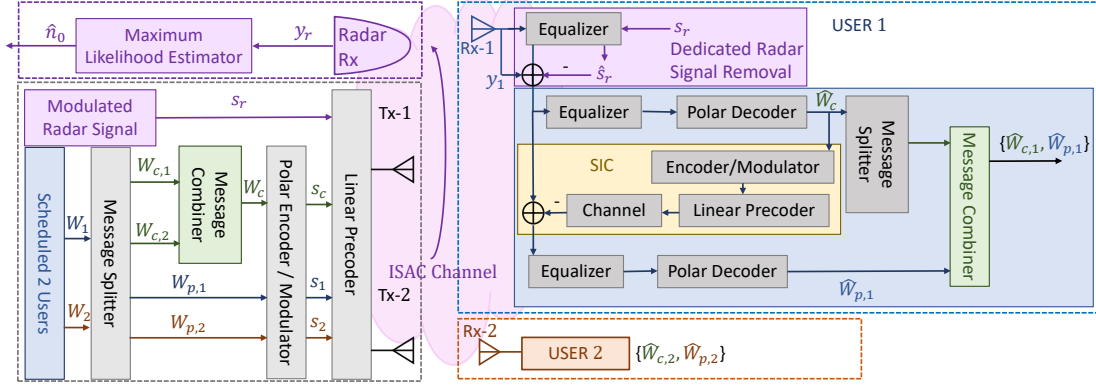


Fig. 1: RSMA ISAC block diagram ($N_T = 2$) implemented using SDRs.

features of the IEEE 802.11ac-VHT physical layer frames [33]:

a) Stage 1: Each TX antenna transmits a pilot signal orthogonally in time comprising a Short Training Field (STF, $12.8\mu\text{s}$ in duration) and a Long Training Field (LTF, $12.8\mu\text{s}$ in duration), as shown in the top portion of Fig. 2. The STF is used for synchronization and coarse frequency offset estimation, while the LTF is used for channel estimation at each UE (i.e., $\hat{\mathbf{h}}_i[k]$)

b) Stage 2: Here, the transmitted signal consists of a preamble followed by the data payload, as shown in the bottom portion of Fig. 2.

- **Preamble:** The preamble consists of one STF and four LTFs. The function of the STF is the same as in Stage 1, while the LTFs are precoded in order to estimate the *precoded channels* for equalization at the UEs. The first LTF is used by UE i to estimate $\mathbf{h}_i^H \mathbf{p}_c$ ($i = 1, 2$) for decoding the common stream ($s_c[\cdot]$). The second LTF is used by UE 1 to estimate $\mathbf{h}_1^H \mathbf{p}_1$ to decode its private stream ($s_1[\cdot]$). Similarly, the third LTF is used by UE 2 to estimate $\mathbf{h}_2^H \mathbf{p}_2$ to decode its private stream ($s_2[\cdot]$). The fourth LTF is used by UE i to estimate $\mathbf{h}_i^H \mathbf{p}_r$ ($i = 1, 2$) in order to subtract the dedicated sensing signal ($s_r[\cdot]$) from (8).
- **ISAC Payload:** For the payload, we consider a total bandwidth of 100MHz with $N_c = 512$ subcarriers and a cyclic prefix (CP) of 128 samples per OFDM symbol. Aligned with IEEE 802.11ac-VHT frames, 468 subcarriers are used to carry data symbols, 16 subcarriers are used to correct the common phase error across all subcarriers in one OFDM symbol [37], and the rest serve as guard bands. This yields an effective bandwidth of:

$$\begin{aligned}
 B &= 100\text{MHz} \times \underbrace{(512/640)}_{\text{CP overhead}} \times \underbrace{(468/512)}_{\text{Guard band overhead}} \\
 &= 73.125\text{MHz}.
 \end{aligned} \tag{20}$$

The ISAC payload consists of at most four superposed streams (one dedicated sensing signal, one common, two private), each comprising 5 OFDM symbols.

- **MCS Implementation:** Table III lists the MCS levels, \mathcal{M} , implemented in our prototype. For channel coding,

MCS Index \mathcal{M}	Modulation (m)	Code Rate r	Data Rate Bmr (Mbps)
0	BPSK (1)	1/2	36.5625
1	BPSK (1)	3/4	54.84375
2	QPSK (2)	1/2	73.125
3	QPSK (2)	3/4	109.6875
4	16QAM (4)	1/2	146.25
5	16QAM (4)	3/4	219.375
6	64QAM (6)	2/3	292.5
7	64QAM (6)	3/4	329.0625
8	256QAM (8)	3/4	438.75
9	256QAM (8)	5/6	487.5

TABLE III: MCS levels (largely based on IEEE 802.11ac-VHT) implemented in our prototype. The data rate in the last column is equal to Bmr , where B is the effective bandwidth given by (20).

we implement Polar codes augmented with an 8-bit cyclic redundancy check [38], [39], along with successive cancellation list decoding [40], with a list depth of 2. After the preamble, the first OFDM symbol (labelled SERVICE in the bottom portion of Fig. 2) contains the MCS information of each stream.

- **Dedicated Sensing Signal:** For $s_r[\cdot]$, we consider a BPSK stream known to the UEs.

IV. EXPERIMENTAL RESULTS

A. Measurement Environment

Our measurements were conducted in a fairly empty lecture room (Fig. 3), where the furniture was moved to the far end of the room, well away from the target, to reduce clutter. We used a metal box (1m high and 0.8m wide) placed at the roadside of the TX antennas to mimic a vehicular target. An anchor antenna was also placed at the TX roadside for phase calibration [41].

We considered three scenarios as described below, capturing different levels of inter-UE interference and separation/integration between comms and sensing:

- S1. **UEs and target mutually well separated** (in the angular domain), as shown in Fig. 3 (left). The larger the separation among UEs in the angular domain, the better SDMA can suppress the inter-UE interference. As a result, the

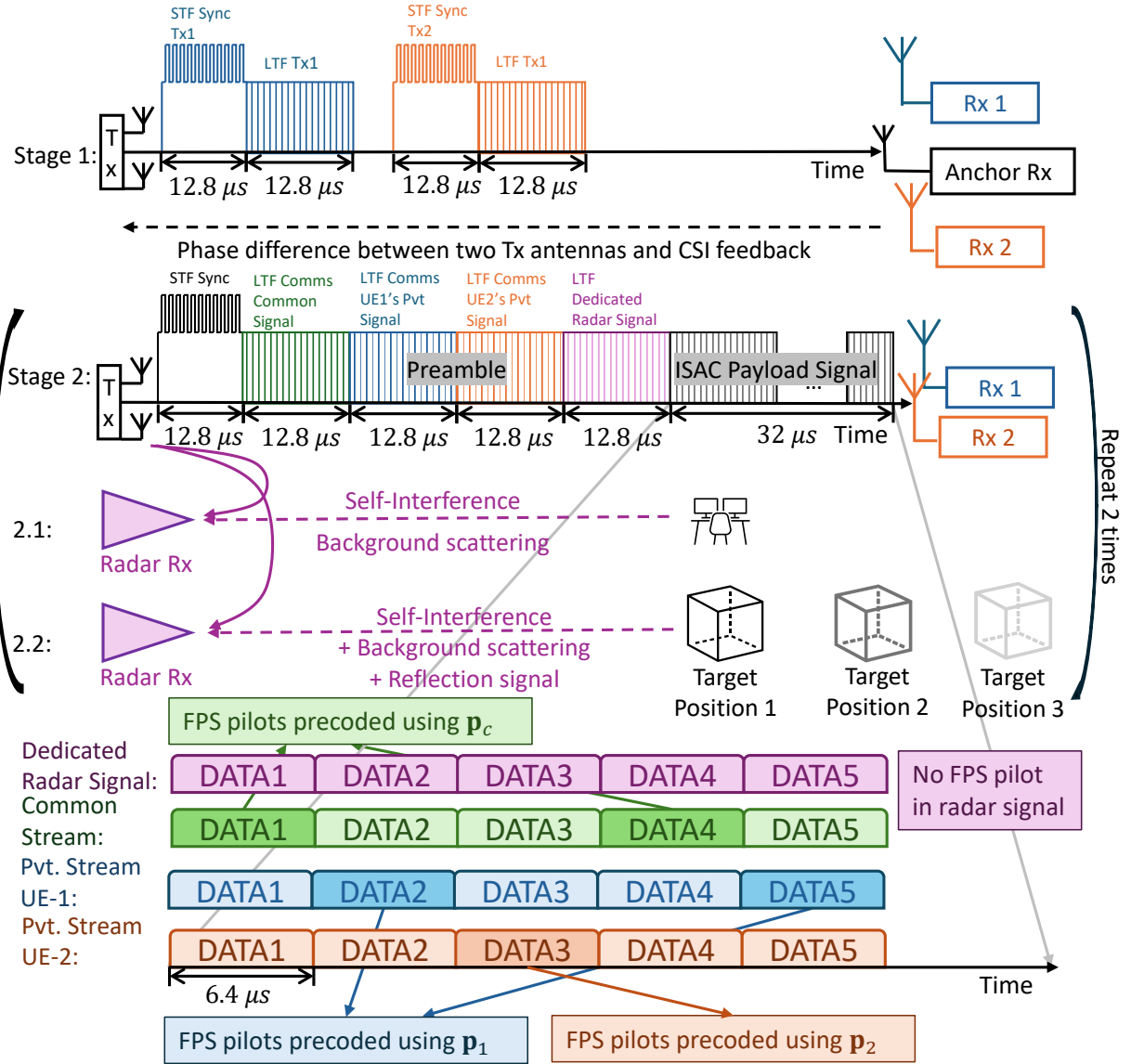


Fig. 2: Signal structure within the two-stage transmission protocol used to implement RSMA ISAC in our prototype. In conventional, SDMA-based 802.11ac-VHT, where each UE has to decode only one data stream, every DATA (OFDM) symbol contains 16 *precoded* pilot subcarriers used to correct phase errors in the estimate of a UE's precoded channel. This protects against decoding errors caused by rotated constellations post equalization, and is known as fine phase shift (FPS) [37]. On the other hand, in RSMA, each UE needs to decode two data streams. To avoid FPS pilot contamination between overlapping streams, we use p_c to precode the FPS pilots in DATA symbols 1 and 4, similarly p_1 in DATA symbols 2 and 5, and p_2 in DATA symbol 3. The FPS pilots are unused in the stream carrying the dedicated radar signal.

RSMA gain – i.e., the extent to which its ISAC performance region is bigger than SDMA's – could potentially be modest. Similarly, the extent of separation/integration between comms and sensing separation is dictated by the angular separation between the UEs and the target. A large angular separation may require a dedicated sensing signal to achieve the RSMA ISAC performance boundary.

- S2. **UEs close together, but well separated from the target**, as shown in Fig. 3 (middle). By allocating more power to the common stream, RSMA can better suppress the high inter-UE interference when the UEs are not adequately separated in the angular domain. Hence, RSMA

is expected to yield large throughput gains over SDMA in this scenario.

- S3. **UEs and targets mutually close together**, as shown in Fig. 3 (right). The high level of integration between comms and sensing and the prominent role played by the common stream in suppressing the inter-UE interference makes this the most likely scenario where a dedicated sensing signal may not be needed for achieving the RSMA ISAC performance boundary.

It is worth pointing out that the geometry of these scenarios are representative of what could be encountered in peer-to-peer vehicular ISAC.

Parameter	Notation	Value
Center frequency	f_c	2.5GHz
Transmit power	P_t	23dBm
Wavelength	λ	0.12m
No. of UEs		2
No. of targets		1
Total bandwidth		100MHz
Subcarriers	Total (N_c)	512
	Data	468
	Pilot (FPS)	16
	Guard band	28
CP length		128
Effective bandwidth	B	73.125MHz
OFDM symbols in payload		5
Range resolution		1.5m
Radar \rightarrow Target distances		2.25m ($n_0 = 1$) 3.75m ($n_0 = 2$) 5.25m ($n_0 = 3$)
TX \rightarrow UE distances		≈ 1.5 m
TX antenna spacing	d	0.0625m
Fraunhofer distance (far-field criterion)		0.065m

TABLE IV: List of miscellaneous parameters in our experiments.

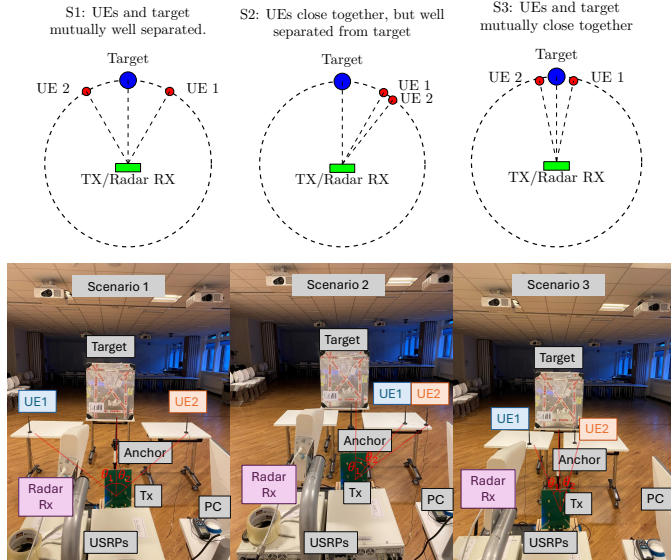


Fig. 3: The three scenarios considered in our measurements.

For each scenario, the goal of our measurements is to empirically characterize the RSMA ISAC performance region as per Definition 1. However, this can be quite cumbersome with four precoder parameters involved in determining each point $(T_{\text{sum}}(\mathbf{P}), \text{SNR}_{\text{rad}}(\mathbf{P}))$ in the RSMA ISAC performance region; for instance, with each parameter taking values over $[0, 1]$, a granularity of 0.1 per parameter yields 10^4 measurements. That said, it is more important to characterize the boundary of the RSMA ISAC performance region than its interior, as the boundary captures the limits of achievable ISAC performance. Thus, Remark 9 motivates the question: can we identify a smaller set of “well-chosen” precoder parameters corresponding to the boundaries of the RSMA and SDMA ISAC performance regions for a given scenario? We address this question next.

B. Simulation-aided search for precoder parameters

Given the estimated UE channels $(\hat{\mathbf{h}}_i[k])$, one can obtain a *simulated* RSMA ISAC performance region via a fine-grained sweep of the precoder parameters. We make this notion precise through the following definition.

Definition 2 (Simulated RSMA ISAC performance region). *The simulated RSMA ISAC performance region is the set of points $(T_{\text{sum}}(\mathbf{P}), G_0(\mathbf{P}))$, where $T_{\text{sum}}(\mathbf{P})$ is the **expected**, rather than measured, sum throughput (see Remark 8), and $G_0(\mathbf{P})$ is the power radiated towards the TX’s broadside, given by*

$$G_0(\mathbf{P}) = \sum_{k=0}^{N_c-1} |\mathbf{a}_0^H \mathbf{x}[k]|^2, \quad (21)$$

In Definition 1, the sensing metric – $\text{SNR}_{\text{rad}}(\mathbf{P})$ – is straightforward to evaluate using measurement data (see 19). However, to evaluate $\text{SNR}_{\text{rad}}(\mathbf{P})$ in a simulation setting, we need to make several (potentially unrealistic) assumptions regarding the radar return (extent of signal attenuation, clutter etc.) which we wish to avoid. Hence, we use $G_0(\mathbf{P})$, which is proportional to $\text{SNR}_{\text{rad}}(\mathbf{P})$, as the sensing metric for the simulated RSMA ISAC performance region.

Ideally, the simulated RSMA ISAC performance region should be a good proxy for the *true* performance region – in particular, the precoder parameters corresponding to the RSMA/SDMA boundaries should have similar values over both regions; this then yields a smaller set of “well-chosen” parameter values that can be used for measuring RSMA and SDMA ISAC performance.

Fig. 4 plots the simulated RSMA ISAC region for each scenario by sweeping over the four precoder parameters in increments of 0.1, resulting in a reasonably comprehensive exploration of the parameter space. The points corresponding to the special cases in Table I are marked as well. The sum throughput values in these plots are based on *measured* UE channels – for each scenario, we placed the UEs approximately 1.5m away from the TX without any target present⁶, and estimated the UE channels through only Stage 1 transmission in Fig. 2. We obtain the following insights from Fig. 4:

a) *Impact of finite MCS levels:* Perhaps the most striking feature of Fig. 4 is the *non-convex* nature of the ISAC performance regions. In particular, the discretized nature of $T_{\text{sum}}(\mathbf{P})$ is a direct consequence of assuming finite MCS levels – instead of a one-to-one mapping between the throughput and SINR (i.e., $\log(1 + \text{SINR})$), a range of SINR values map to the same $T_{\text{sum}}(\mathbf{P})$.

⁶Indeed, the UE channels are affected by the target, which contributes a multipath component (TX \rightarrow Target \rightarrow UE) whose strength depends on the target range. However, for channels of similar strength, as in each of our scenarios, $T_{\text{sum}}(\mathbf{P})$ is chiefly determined by the spatial correlation between the channels, which dictates the amount of inter-UE interference. The spatial correlation is not too sensitive to the target range; in fact, it remains qualitatively unchanged (i.e., low in S1, high in S2 and S3) even without a target. Thus, measuring the UE channels without a target present allows for the convenience of generating a single simulated RSMA ISAC performance region per scenario that is an effective proxy for the true performance region, regardless of the target range.

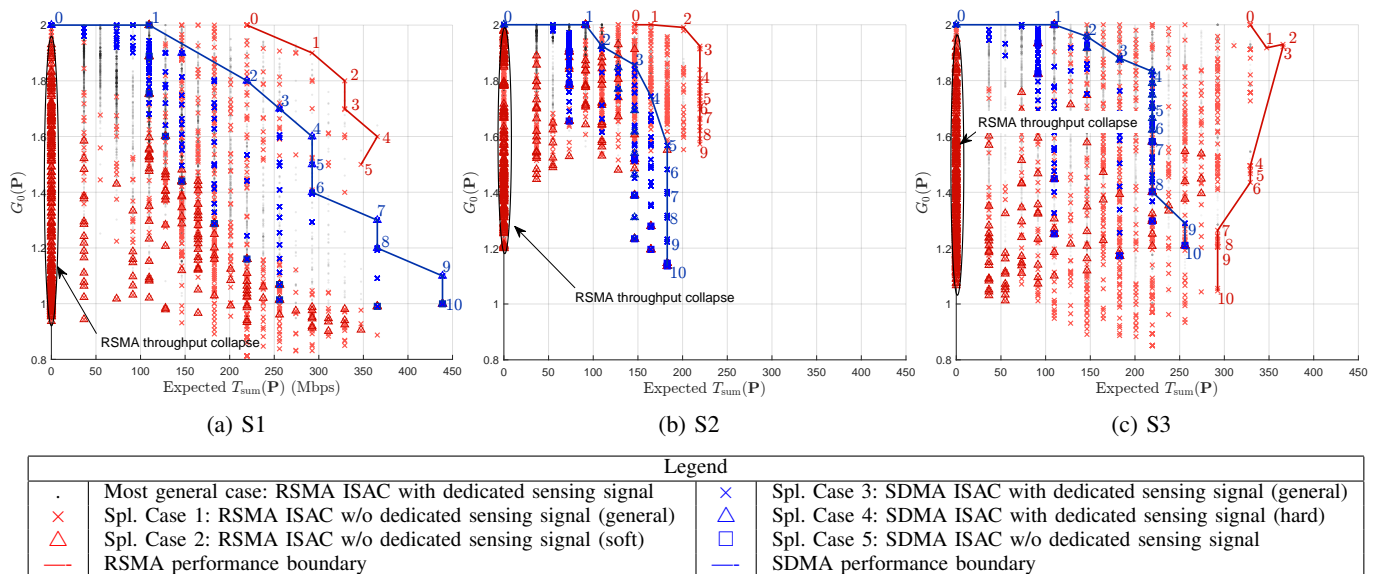


Fig. 4: Simulated RSMA ISAC performance regions, as per Definition 2, for each of the scenarios in Fig. 3. The parameters associated with the points (marked 0, 1, etc.) on the SDMA and RSMA performance boundaries are listed in Table V.

b) Impact of imperfect SIC: A significant proportion of RSMA points lie on the y -axis, where $T_{\text{sum}}(\mathbf{P}) = 0$. These capture the *throughput collapse* phenomenon, where for at least one of the UEs, the SINR is insufficient to decode the common stream at the lowest MCS level in Table III (see also Remark 6). Throughput collapse also explains why the RSMA ISAC performance boundary does not extend as far down as the SDMA boundary in the southeast region of Figs. 4a-b. The common stream SINR reduces as we move from northwest to southeast along the RSMA boundary; when it becomes low enough to trigger a throughput collapse, the boundary ends abruptly.

c) Impact of Interference: In scenarios S2 and S3, the peak (expected) SDMA sum throughput reduces by more than half relative to S1, due to the much higher inter-user interference caused by the proximity of the users.

d) RSMA ISAC outperforms SDMA ISAC: The SDMA ISAC performance boundary lies in the interior of the RSMA ISAC performance region, thereby addressing the second question posed in Remark 9. Hence, for well-chosen precoders (which boils down to well-chosen parameters), RSMA ISAC achieves points in the northeast region beyond the SDMA boundary. Furthermore, the extent to which RSMA ISAC outperforms SDMA ISAC is scenario dependent. In scenario S1, where there is a relatively larger angular separation between the UEs, the gap between the RSMA and SDMA boundaries is narrower. The gap becomes much wider – especially around the northeast corner – as the UEs move closer together in S2 and S3⁷.

⁷In Fig. 4c, only points 0 to 3 should be considered representative of RSMA's performance boundary for achieving desirable outcomes. The red boundary points from 4 to 10 fall outside the effective performance boundary for RSMA in ISAC evaluation, as their parameter settings cause both $T_{\text{sum}}(\mathbf{P})$ and $G_0(\mathbf{P})$ to decrease. We continue to measure these points because they represent the easternmost extent of the red points.

e) RSMA ISAC performance boundary achieved without a dedicated sensing signal: In each scenario, the points on the RSMA ISAC performance boundary are achieved when $t_{\text{comms}} = 1$, which corresponds to special case 1 in Table I where the entire transmit power is allocated for comms. This insight addresses the first question posed in Remark 9.

f) Dedicated sensing signal needed to achieve SDMA ISAC performance boundary: Unlike in d), the points corresponding to SDMA ISAC without a dedicated sensing signal (i.e., special case 5 in Table I) do not lie on the SDMA ISAC performance boundary.

Next, we seek to validate the above insights through measurements by selecting precoder parameters listed in Table V associated with the SDMA and RSMA ISAC boundary points marked 0, 1, etc., in Fig. 4.

C. Measurements

We conducted a total of 180 measurements with the following breakdown:

- RSMA – 81 measurements (6 boundary points for S1, 10 for S2 and 11 for S3, along with 3 different target ranges per boundary point to evaluate the effectiveness of ranging, especially for RSMA without a dedicated sensing signal; more details in paragraph a) below).
- SDMA – 99 measurements (11 boundary points each for S1, S2 and S3, along with 3 different target ranges per boundary point).

In these measurements, the UE locations were unchanged from the ones used to obtain Fig. 4. To suppress the radar self-interference (i.e., signal propagation along the direct path from the TX to the radar RX) and background clutter, we perform a simple background subtraction, where Stage 2 is repeated twice per measurement (illustrated as Stages 2.1 and 2.2 in Fig. 2). In the first instance, we obtain the radar return without

Meas. Index	S1				S2				S3			
	t_{comms}	α_p	\mathcal{M}_1	\mathcal{M}_2	t_{comms}	α_p	\mathcal{M}_1	\mathcal{M}_2	t_{comms}	α_p	\mathcal{M}_1	\mathcal{M}_2
0	0	-	-	-	0	-	-	-	0	-	-	-
1	0.1	1	0	0	0.1	0.8	0	0	0.4	0	0	0
2	0.2	1	1	1	0.2	0.8	0	0	0.1	1	0	0
3	0.3	1	1	2	0.3	0.8	0	0	0.2	0.9	0	0
4	0.4	1	3	3	0.4	0.8	1	1	0.4	1	1	1
5	0.5	1	3	3	0.5	0.8	1	1	0.5	0.9	1	1
6	0.6	1	3	4	0.6	0.8	1	1	0.6	0.9	1	1
7	0.7	1	3	4	0.7	0.8	1	1	0.9	0.7	1	1
8	0.8	1	3	4	0.8	0.8	1	1	1	0.7	1	1
9	0.9	1	3	4	0.9	0.8	1	1	1	0.9	2	2
10	1	1	4	4	1	1	2	2	1	1	2	2

(a) SDMA ($t_p = 1$)

Meas. Index	S1						S2						S3					
	t_p	α_c	α_p	\mathcal{M}_c	\mathcal{M}_1	\mathcal{M}_2	t_p	α_c	α_p	\mathcal{M}_c	\mathcal{M}_1	\mathcal{M}_2	t_p	α_c	α_p	\mathcal{M}_c	\mathcal{M}_1	\mathcal{M}_2
0	0	1	1	5	-	-	0	0	0	4	-	-	0	0	0	5	-	-
1	0.1	1	1	3	0	0	0.2	0	0.2	2	0	0	0.1	0	0.6	4	0	0
2	0.2	1	1	2	1	1	0.2	0	0.3	2	0	0	0.1	0	0.8	4	0	0
3	0.3	1	1	1	3	3	0.2	0	0.4	2	0	0	0.1	0	0.7	3	0	0
4	0.4	1	1	0	3	3	0.2	0	0.5	2	0	0	0	1	1	5	-	-
5	0.5	1	1	0	3	5	0.2	0	0.6	1	0	0	0.3	1	0.9	3	1	1
6	-	-	-	-	-	-	0.2	0	0.7	1	1	1	0.3	1	0.8	3	0	0
7	-	-	-	-	-	-	0.2	1	0.4	3	0	0	0.3	0.9	0.9	3	1	1
8	-	-	-	-	-	-	0.2	1	0.6	2	0	1	0.1	0.9	1	4	0	0
9	-	-	-	-	-	-	0.2	1	0.7	3	0	1	0	0.9	1	4	1	1
10	-	-	-	-	-	-	-	-	-	-	-	-	0.1	0.8	0.7	3	0	0

(b) RSMA without dedicated sensing signal ($t_{\text{comms}} = 1$)

TABLE V: Precoder parameters associated with the boundary points of the simulated ISAC performance regions in Fig. 4 (the numbers marked 0, 1, and so on, in Fig. 4 correspond to the measurement index in the first column). The MCS levels shown are the ones that maximize the *expected* sum throughput, based on Remark 5. These parameters are used for our measurements in Section IV-C.

any target present (Stage 2.1) to capture only the radar self-interference and any background clutter. This signal is then subtracted from the radar return obtained when the target is present (Stage 2.2). Table V lists the miscellaneous parameters used in our measurements.

a) *Ranging performance of RSMA ISAC without a dedicated sensing signal*: The 100MHz signal bandwidth yields a range resolution of 1.5m. Hence, in our measurements, we considered target ranges of 2.25m ($n_0 = 1$), 3.75m ($n_0 = 2$) and 5.25m ($n_0 = 3$) for each scenario, corresponding to the middle of the second, third and fourth range bins, respectively⁸, as shown in Fig. 5.

For scenario S1, Fig. 6 compares the ranging performance of RSMA (without a dedicated sensing signal) and SDMA (with a dedicated sensing signal). The heatmaps plot $\text{SNR}_{\text{rad}}(\mathbf{P})$ for each range bin. In each heatmap, the target is clearly identifiable at the correct range bin. Moreover, there is a graceful degradation in $\text{SNR}_{\text{rad}}(\mathbf{P})$ with increasing n_0 (left to right along each row), consistent with a progressively weaker radar return. Importantly, the absence of a dedicated sensing signal for RSMA does not adversely impact its ranging performance. The heatmaps for scenarios S2 and S3 look similar and hence, not presented.

b) *Measured ISAC performance region – RSMA v/s SDMA*: For the target situated at 5.25m ($n_0 = 3$), Fig. 7 plots the measured ISAC performance region for the precoder

⁸ $n_0 = 0$ corresponds to the first range bin.

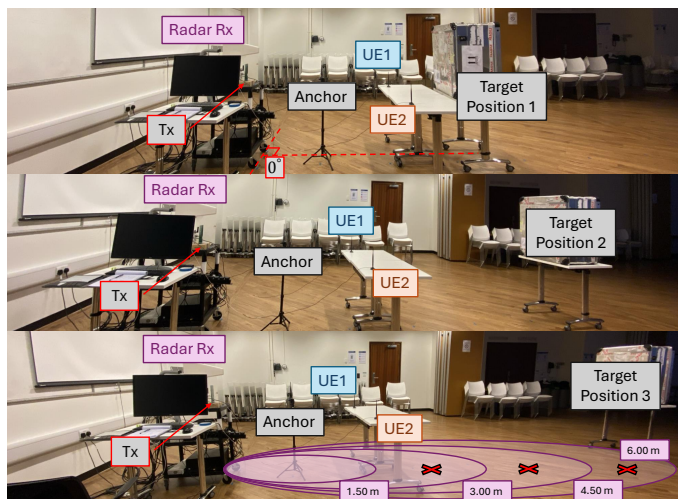


Fig. 5: The three target distances considered for each scenario in Fig. 3 – 2.25m (top), 3.75m (middle) and 5.25m (bottom), which corresponds to the middle of the second ($n_0 = 1$), third ($n_0 = 2$) and fourth ($n_0 = 3$) range bins, respectively. The 100MHz signal bandwidth yields a range resolution (bin size) of 1.5m, which is marked in the bottom figure.

parameters listed in Table V. To measure $T_{\text{sum}}(\mathbf{P})$, we identified the highest MCS levels that resulted in error-free decoding of the five OFDM symbols in the data payload (see Fig. 2) by using the MCS levels in Table V as a starting

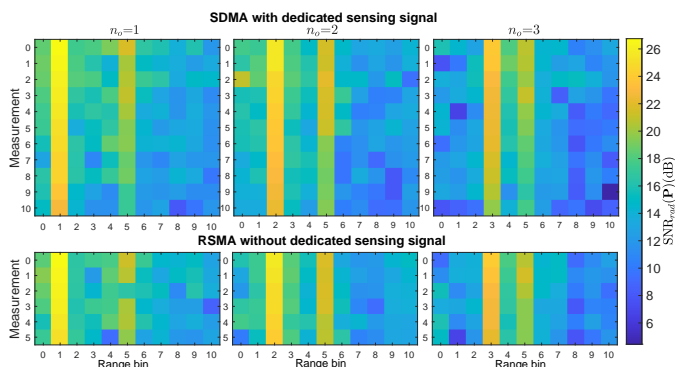


Fig. 6: Heatmap plotting the measured $\text{SNR}_{\text{rad}}(\mathbf{P})$ for scenario S1 across three different target distances – 2.25m ($n_0 = 1$), 3.75m ($n_0 = 2$) and 5.25m ($n_0 = 3$). (Top row): SDMA with a dedicated sensing signal; (bottom row) RSMA without a dedicated sensing signal. The y -axis in each heatmap corresponds to the measurement index in Table V. RSMA without a dedicated sensing signal achieves a ranging performance comparable to SDMA with a dedicated sensing signal.

point and progressively decreasing/increasing the MCS levels if there were any/no decoding errors. Hence, any difference between the expected $T_{\text{sum}}(\mathbf{P})$ in Fig. 4 and the measured $T_{\text{sum}}(\mathbf{P})$ in Fig. 7 boils down to a mismatch between the initial MCS levels in Table V-b and ones that maximized the measured sum throughput.

The following aspects of Fig. 4 are validated by Fig. 7:

- *RSMA ISAC empirically outperforms SDMA ISAC*: Except for point 5 in S1, all other RSMA measurement points lie to the northeast of the SDMA ISAC performance boundary. Consistent with the heatmaps from Fig. 6, the measured $\text{SNR}_{\text{rad}}(\mathbf{P})$ is comparable for both SDMA and RSMA, varying between 20 to 24dB. The gain in peak throughput for RSMA over SDMA is:
 - S1: –6% (SDMA: 292.5Mbps, RSMA: 274Mbps)
 - S2: 12% (SDMA: 146.25Mbps, RSMA: 164Mbps)
 - S3: 50% (SDMA: 146.25Mbps, RSMA: 219Mbps)

Despite the caveat that our measured throughput is based on the decoding of only five OFDM symbols, we still notice the SDMA sum throughput dropping by half for S2 and S3, relative to S1, due to the high inter-user interference, consistent with Fig. 4.

- *RSMA throughput collapse due to imperfect SIC and finite MCS levels*: For point 5 (RSMA) in S1, the common stream cannot be decoded even at the lowest MCS level (BPSK rate 1/2), possibly due to large CSI estimation errors. Hence, imperfect SIC causes throughput collapse.

Finally, the main aspect in which Fig. 7 differs from Fig. 4 is the absence of a clear RSMA performance boundary. This is due to the mismatch between the MCS levels in Table V-b and the ones that maximize the measured sum throughput for a given RSMA point. In particular, if the common stream cannot be decoded at the MCS level in Table V-b, it results in a lower measured sum throughput than in Fig. 4. An extreme example of this is RSMA point 5 in Fig. 7a, where the common stream cannot be decoded at the lowest MCS level ($\mathcal{M}_c = 0$),

which in turn causes throughput collapse. Since the measured RSMA throughput is based on the decoding of only five OFDM symbols per stream, there is no systematic pattern to this MCS level mismatch. This issue can be addressed through larger payloads and link adaptation, yielding a long-term average measured throughput that should make the RSMA performance boundary clearer. This can be the subject of ongoing work.

V. CONCLUSION

In this paper, we presented the first ever experimental study of RSMA ISAC using SDRs. We started by formulating signal model that included four different ISAC precoder design choices – RSMA/SDMA with/without dedicated sensing signal – as special cases. Using sum throughput as the comms metric and (post-processing) radar SNR as the sensing metric, we defined the ISAC performance region to evaluate these design choices. Over three measurement scenarios that are representative of vehicular ISAC, involving communicating with two users and ranging a single target with different levels of inter-user interference and separation/integration between sensing and communications, we observed that RSMA has a larger ISAC performance region than SDMA. Notably, RSMA without a dedicated sensing signal outperformed SDMA with a dedicated sensing signal, by achieving peak sum throughput gains of upto 50% for similar radar SNR (between 20 and 24dB).

Though further enhancement of this prototype is possible by incorporating link adaptation, our results provide compelling answers to questions Q1 and Q2 posed on page 1 – i.e., *RSMA without a dedicated sensing signal achieves better ISAC performance than SDMA with a dedicated sensing signal*.

REFERENCES

- [1] “Technical Specification Group TSG SA; Service requirement for Integrated Sensing and Communications (release 19),” TS 22.137 (v0.1.0), 3GPP, Aug. 2023.
- [2] F. Liu *et al.*, “Integrated sensing and communications: Toward dual-functional wireless networks for 6G and beyond,” *IEEE J. Sel. Areas Commun.*, vol. 40, no. 6, pp. 1728–1767, 2022.
- [3] B. Clerckx *et al.*, “Multiple Access Techniques for Intelligent and Multifunctional 6G: Tutorial, Survey, and Outlook,” *Proceedings of the IEEE*, vol. 112, no. 7, pp. 832–879, 2024.
- [4] X. Liu *et al.*, “Joint transmit beamforming for multiuser MIMO communications and MIMO radar,” *IEEE Trans. Signal Process.*, vol. 68, pp. 3929–3944, 2020.
- [5] F. Liu *et al.*, “Cramér-Rao bound optimization for joint radar-communication beamforming,” *IEEE Trans. Signal Process.*, vol. 70, pp. 240–253, 2022.
- [6] S. Lu *et al.*, “Random ISAC signals deserve dedicated precoding,” *IEEE Trans. Signal Process.*, vol. 72, pp. 3453–3469, 2024.
- [7] Y. Cui *et al.*, “Optimal precoding design for monostatic ISAC systems: MSE lower bound and DoF completion,” in *Proc. of the IEEE Wireless Commun. and Networking Conf. (WCNC)*, 2024, pp. 1–6.
- [8] Z. Liu, S. Aditya, H. Li, and B. Clerckx, “Joint transmit and receive beamforming design in full-duplex integrated sensing and communications,” *IEEE J. Sel. Areas Commun.*, vol. 41, no. 9, pp. 2907–2919, 2023.
- [9] Y. Fan, S. Wu, X. Bi, and G. Li, “Power allocation for cell-free Massive MIMO ISAC systems with OTFS signal,” *IEEE Internet Things J.*, pp. 1–1, 2024.
- [10] B. Liao, H. Q. Ngo, M. Matthaiou, and P. J. Smith, “Power allocation for massive MIMO-ISAC systems,” *IEEE Trans. Wireless Commun.*, vol. 23, no. 10, pp. 14 232–14 248, 2024.

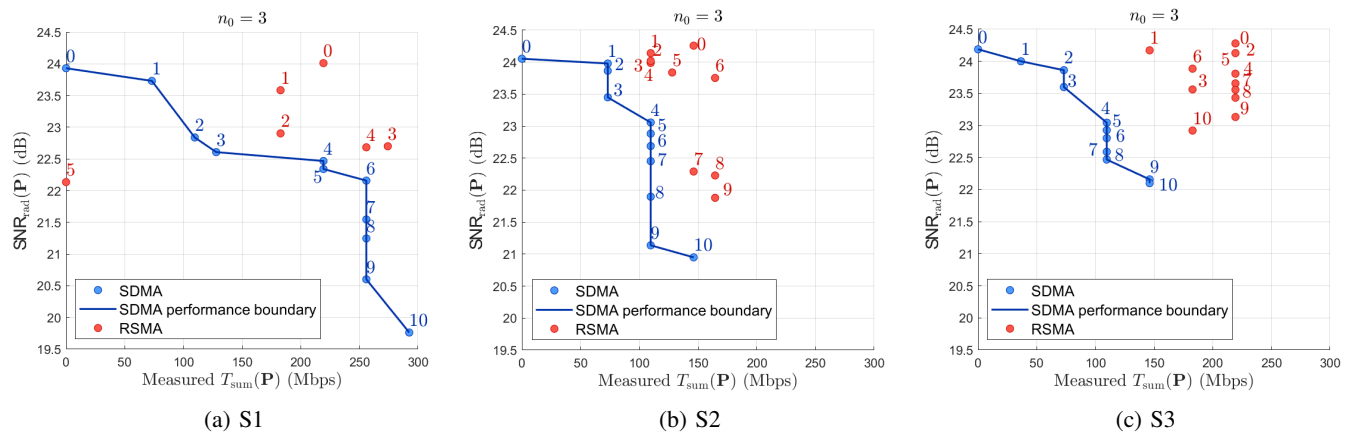


Fig. 7: The measured ISAC performance region for RSMA and SDMA, for the precoder parameters in Table V. The MCS levels in Table V are used as a starting point and progressively decreased/increased the MCS levels in case of any/no decoding errors. Hence, any difference between the expected $T_{\text{sum}}(\mathbf{P})$ in Fig. 4 and the measured $T_{\text{sum}}(\mathbf{P})$ in Fig. 7 boils down to a mismatch between the initial MCS levels in Table V and ones that maximized the measured sum throughput.

- [11] O. A. Topal, T. Demir, E. Björnson, and C. Cavdar, “Multi-target integrated sensing and communications in massive MIMO systems,” *IEEE Wireless Commun. Lett.*, pp. 1–1, 2024.
- [12] U. Demirhan and A. Alkhateeb, “Learning beamforming in cell-free Massive MIMO ISAC systems,” in *2024 IEEE 25th International Workshop on Signal Processing Advances in Wireless Communications (SPAWC)*, 2024, pp. 326–330.
- [13] F. Liu, W. Yuan, C. Masouros, and J. Yuan, “Radar-assisted predictive beamforming for vehicular links: Communication served by sensing,” *IEEE Trans. Wireless Commun.*, vol. 19, no. 11, pp. 7704–7719, 2020.
- [14] W. Yuan *et al.*, “Bayesian predictive beamforming for vehicular networks: A low-overhead joint radar-communication approach,” *IEEE Trans. Wireless Commun.*, vol. 20, no. 3, pp. 1442–1456, 2021.
- [15] C. Qi, W. Ci, J. Zhang, and X. You, “Hybrid beamforming for millimeter wave MIMO integrated sensing and communications,” *IEEE Commun. Lett.*, vol. 26, no. 5, pp. 1136–1140, 2022.
- [16] X. Wang, Z. Fei, J. A. Zhang, and J. Xu, “Partially-connected hybrid beamforming design for integrated sensing and communication systems,” *IEEE Trans. Commun.*, vol. 70, no. 10, pp. 6648–6660, 2022.
- [17] A. Gupta *et al.*, “An affine precoded superimposed pilot-based mmwave MIMO-OFDM ISAC system,” *IEEE Open Journal of the Communications Society*, vol. 5, pp. 1504–1524, 2024.
- [18] P. Wang *et al.*, “Low-complexity joint transceiver optimization for MmWave/THz MU-MIMO ISAC systems,” *IEEE Internet Things J.*, pp. 1–1, 2024.
- [19] Q. Lin *et al.*, “One-bit transceiver optimization for mmwave integrated sensing and communication systems,” *IEEE Trans. Commun.*, pp. 1–1, 2024.
- [20] X. Lyu, S. Aditya, J. Kim, and B. Clerckx, “Rate-Splitting Multiple Access: The First Prototype and Experimental Validation of its Superiority over SDMA and NOMA,” *IEEE Trans. Wireless Commun.*, vol. 23, no. 8, Aug. 2024.
- [21] X. Lyu, S. Aditya, and B. Clerckx, “Rate-Splitting Multiple Access for overloaded multi-group multicast: A first experimental study,” *IEEE Trans. Broadcast.*, Oct. 2024, (Early Access).
- [22] B. Clerckx *et al.*, “A Primer on Rate-Splitting Multiple Access: Tutorial, Myths, and Frequently Asked Questions,” *IEEE J. Sel. Areas Commun.*, vol. 41, no. 5, pp. 1265–1308, May 2023.
- [23] S. Aditya, O. Dizdar, B. Clerckx, and X. Li, “Sensing using coded communications signals,” *IEEE Open Journal of the Communications Society*, vol. 4, pp. 134–152, 2023.
- [24] C. Xu *et al.*, “Rate-splitting multiple access for multi-antenna joint radar and communications,” *IEEE J. Sel. Topics Signal Process.*, vol. 15, no. 6, pp. 1332–1347, 2021.
- [25] Z. Liu, Y. Jint, B. Cao, and R. Lu, “RISAC: Rate-Splitting Multiple Access enabled Integrated Sensing and Communication systems,” in *Proc. of the IEEE Intl. Conf. on Commun. (ICC)*, 2023, pp. 6449–6454.
- [26] Z. Liu, L. Yin, W. Shin, and B. Clerckx, “Rate-splitting multiple access for quantized ISAC LEO satellite systems: A max-min fair energy-efficient beam design,” *IEEE Trans. Wireless Commun.*, vol. 23, no. 10, pp. 15394–15408, 2024.
- [27] R. C. Loli, O. Dizdar, and B. Clerckx, “Rate-Splitting Multiple Access for multi-antenna joint radar and communications with partial CSIT: Precoder Optimization and Link-Level simulations,” 2022. [Online]. Available: <https://arxiv.org/abs/2201.10621>
- [28] L. Yin, Y. Mao, O. Dizdar, and B. Clerckx, “Rate-splitting multiple access for 6G—Part II: Interplay with integrated sensing and communications,” *IEEE Commun. Lett.*, vol. 26, no. 10, pp. 2237–2241, 2022.
- [29] S. Ding *et al.*, “Integrated Sensing and Communication: Prototype and Key Processing Algorithms,” in *Proc. of the IEEE Intl. Conf. on Commun. (ICC) Workshops*, 2023, pp. 225–230.
- [30] —, “Channel measurements for integrated sensing and communication: Method and prototype test,” in *Proc. of the 99th IEEE Vehicular Tech. Conf. (VTC-Spring)*, 2024, pp. 01–06.
- [31] M. Ouyang, Y. Wang, T. Zhang, and F. Gao, “An RFSoc-based scalable ISAC prototyping platform with OTFS waveform,” in *Proc. of the IEEE Wireless Commun. and Netw. Conf. (WCNC)*, 2024, pp. 1–5.
- [32] T. Xu, F. Liu, C. Masouros, and I. Darwazeh, “An experimental proof of concept for integrated sensing and communications waveform design,” *IEEE Open Journal of the Communications Society*, vol. 3, pp. 1643–1655, 2022.
- [33] “IEEE Standard for Information technology - Telecommunications and information exchange between systems - local and metropolitan area networks -specific requirements - part 11: Wireless LAN Medium Access Control (MAC) and Physical Layer (PHY) Specifications—Amendment 4: Enhancements for very high throughput for operation in bands below 6 GHz,” *IEEE Std 802.11ac (TM) - 2013*, pp. 1–425, 2013.
- [34] P. Mogensen *et al.*, “LTE capacity compared to the Shannon bound,” in *Proc. of the 65th IEEE Vehicular Tech. Conf. (VTC Spring)*, 2007, pp. 1234–1238.
- [35] X. Lyu, S. Aditya, and B. Clerckx, “Rate-splitting Multiple Access for Non-Orthogonal Unicast Multicast: An experimental study,” in *Proc. of the 25th IEEE Intl. Workshop on Signal Proc. Advances in Wireless Commun. (SPAWC)*, 2024, pp. 591–595.
- [36] H. Joudeh and B. Clerckx, “Sum-rate maximization for linearly precoded downlink multiuser MISO systems with partial CSIT: A rate-splitting approach,” *IEEE Trans. Commun.*, vol. 64, no. 11, pp. 4847–4861, 2016.
- [37] H. Minn, “A robust timing and frequency synchronization for OFDM systems,” *IEEE Trans. Wireless Commun.*, vol. 2, no. 4, pp. 822–839, 2003.
- [38] P. Trifonov, “Efficient Design and Decoding of Polar Codes,” *IEEE Trans. Commun.*, vol. 60, no. 11, pp. 3221–3227, 2012.
- [39] H. Li and J. Yuan, “A Practical Construction Method for Polar Codes in AWGN Channels,” in *IEEE 2013 Tencon - Spring*, 2013, pp. 223–226.
- [40] I. Tal and A. Vardy, “List Decoding of Polar Codes,” *IEEE Trans. Inf. Theory*, vol. 61, no. 5, pp. 2213–2226, 2015.
- [41] L. Storrer *et al.*, “Experimental implementation of a multi-antenna 802.11ax-based passive bistatic radar for human target detection,” in *Proc. of the IEEE Radar Conf. (RadarConf20)*, 2020, pp. 1–6.